THE JOURNAL OF PHYSICAL CHEMISTRY C
A JOURNAL OF THE AMERICAN CHEMICAL SOCIETY

pubs.acs.org/JPCC
Article

The Electron−Phonon Interaction at the (110) Surface of Hydrogen-Covered $Mo_{1-x}Re_x$ Alloys from Helium Atom Scattering

Giorgio Benedek, Björn Flach, Joseph R. Manson, Salvador Miret-Artés,* and J. Peter Toennies

Cite This: J. Phys. Chem. C 2025, 129, 17632−17642

ABSTRACT: The electron−phonon interaction (or mass-enhancement (ME) factor) at the hydrogen-covered (110) surface of $Mo_{1-x}Re_x$ alloys has been derived for three different Re concentrations, x = 0.05, 0.15, 0.25, from the incident-energy dependence of Helium atom scattering (HAS) intensities. It is shown that the ME factor may also be extracted, in the case of stepped surfaces, from the maxima of the drift spectra, as well as from the intensities of the diffuse elastic peak and of the inelastic scattering from Rayleigh waves. It is confirmed that the ME factor, and therefore the superconducting critical temperature, increase with Re concentration, together with the charge-density wave gap occurring in the hole−electron dispersion curve of the quasi-one-dimensional free electron gas, observed long ago with inelastic HAS in H-covered $Mo_{1-x}Re_x$ alloys.

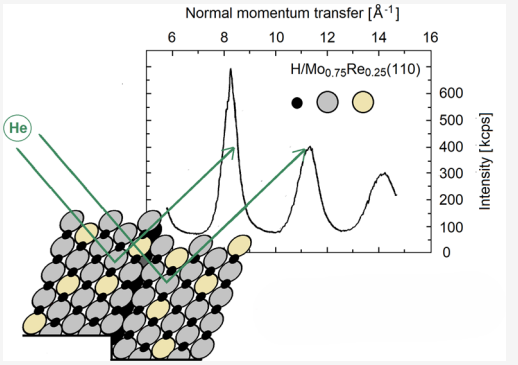

1. INTRODUCTION

The inclusion of hydrogen in superconducting materials has been shown to produce important effects on their properties, in particular, on their critical temperature T_c.[1] The search for superconductors with T_c approaching room temperature has received great impetus in the recent years from metal hydrides, albeit, so far, at very high pressures.[2,3] Within BCS theory, hydrogen has the merit of introducing high frequencies into the phonon spectrum and an increase of the electron−phonon (EP) interaction (mass-enhancement (ME) factor λ[4]). On the other hand, the expected advantages (both physical and nanotechnological) of working with quasi-2D systems has led to the consideration of superlattices made of a hydrogen monolayer interstitially inserted into metal monolayers.[5] In this configuration, comparatively high critical temperatures have been predicted for a $(Be_4)_2H$ superlattice at ambient pressure.[5]

Similar configurations may be conceived for those transition metals and their alloys that are conventional low-temperature superconductors, but do not form stable hydrides at ordinary pressures, such as transition metals and their alloys of groups 6−7.[1] However, some surfaces of these materials, like the (110) surface of W, Mo and Mo−Re alloys, when covered with hydrogen, have been found with helium atom scattering (HAS) to exhibit giant Kohn anomalies in the surface phonon dispersion.[6−11] Such giant anomalies do not occur for the respective clean surfaces and have therefore been considered as signatures of an increased EP interaction due to hydrogen adsorption and additional surface electron band nesting at the Fermi surface. The interest for these superconducting alloys, dating back to the early efforts to raise T_c in metastable films,[12,13] has been revived in the past decade in connection with multiband superconductivity.[14−19] However, no specific study of enhanced surface superconductivity induced by hydrogen adsorption is available to our knowledge.

In the present work, the ME factor for the hydrogen-covered (110) surface of the $Mo_{1-x}Re_x$ alloys (x = 0, 0.05, 0.15, 0.25) is obtained from the Debye−Waller (DW) exponent for both specular and diffuse elastic HAS. The method relies on the fact that for a conducting surface He atoms at thermal energies (<100 meV) are scattered by the free-electron gas a few Å away from the first atomic layer, and therefore the exchange of energy and momentum with lattice vibrations can only occur through the EP coupling, i.e., via the phonon-induced dynamical modulation of the surface charge density.[20,21] Previous applications of the method to superconductor surfaces can be found in refs 20−23. In the case of hydrogen-covered superconductor Mo alloys discussed in the present work, the ME factor is found to increase substantially with the Re concentration, similarly to what is known to occur for the bulk material.[15,24] Moreover, the comparison between ME factor values for the H-covered and the clean surfaces, derived from the same HAS method and only available for

Received: June 12, 2025
Revised: August 23, 2025
Accepted: August 25, 2025
Published: September 16, 2025

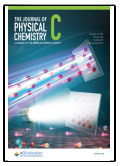

$Mo_{0.95}Re_{0.05}$, shows a significant increase induced by hydrogen adsorption.

2. HAS DIFFRACTION SPECTRA

The HAS diffraction experiments from the clean and hydrogen-covered (110) surfaces of the $Mo_{1-x}Re_x$ alloys, from which the surface EP interaction is derived below, have been reported previously and thoroughly discussed in refs 10 and 11. A description of the HAS apparatus is given in refs 6−10. The scattering chamber operated at ultrahigh vacuum conditions, with a background pressure in the low 10^{-11} mbar range and the sample surface monitored with in situ low-energy electron diffraction (LEED) and Auger electron spectroscopy (AES). A highly expanded He nozzle-beam and a time-of-flight (TOF) spectrometer permit together a high-resolution angular (∼0.1°) and energy (∼2%) spectroscopy of the scattered He atoms. For H-covered surfaces the saturation coverage corresponding to one monolayer (1 ML) was achieved at H-exposures exceeding 10 L at room temperature. The method is described in detail in refs 6−10.

Angular distribution and inelastic time-of flight (TOF) HAS measurements have been performed at a surface temperature of T = 500 K for the clean surfaces and at T = 130 K for the surfaces saturated by one monolayer of hydrogen.[6−10] At these respective temperatures, the clean as well as the 1 ML H-covered surfaces could be kept at constant conditions during a measurement time of up to about 2 h, with no significant perturbing hydrogen adsorption/desorption processes. In what follows, the surface parameters used in the derivation of the EP coupling, namely, the surface unit cell area and the work function, and therefore the EP coupling itself, are those at the actual temperature and H-coverage used in experiments.

The structure of clean surfaces, as originally analyzed by LEED, was reported to be unreconstructed (1 × 1) at all four considered values of Re concentration, x = 0, 0.05, 0.15, and 0.25, with the surface concentration of Re being about that of the bulk.[25]

The higher surface sensitivity of HAS diffraction does, however, provide hints about a weak surface reconstruction at the lower Re concentrations, such as (2 × 2) for x = 0.05 and c(2 × 2) for x = 0.15 (Figure 1a), similar to that observed by Okada et al.[25] with LEED at the same Re concentrations and hydrogen coverage of 0.25 and 0.5 monolayers, respectively. This can be appreciated from the HAS diffraction spectra measured for x = 0.05 (Figures 2a and 3a), and x = 0.15 (Figure 4a,b), with an incident energy E_i = 36.9 meV along the $\bar{\Gamma}\bar{S}$ and $\bar{\Gamma}\bar{N}$ symmetry directions, and E_i = 34.4 meV along $\bar{\Gamma}\bar{H}$ (cfr. Figure 1b,c). In the first case (x = 0.05), in addition to the peaks $\bar{\Gamma}$, corresponding to the (1 × 1) surface structure, weaker peaks are observed. They are labeled S (corresponding in Figure 2a to the S points at the boundaries of the (1 × 1) Brillouin zone (BZ), represented in Figure 1c), and $\bar{N}$ (cfr. Figure 3a). This defines a (2 × 2) reconstruction, with a unit cell four times larger than that of the (1 × 1) surface (Figure 1a).

The diffraction spectrum of Figure 3b also shows weak features (better appreciated in the ×3 magnification) at the wavevectors $\pm Q_{s1} \cong \pm 1$ Å^{-1} and N + $Q_{s1} \cong 3$ Å^{-1}. The comparison with the inelastic HAS data reported by Okada et al.[11] permits to identify the wavevector Q_{s1} with the critical wavevector of the quasi-1D free electron gas induced by the H-coverage (cfr. previous Section). At the critical wavevector the hole−electron dispersion curve of the quasi-1D electron gas

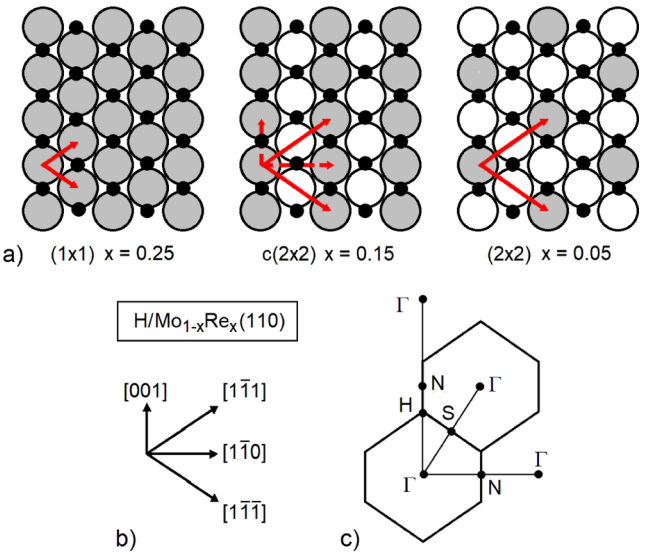

Figure 1. (a) The $Mo_{1-x}Re_x$ (110) surface (large gray and white circles) covered with a hydrogen monolayer (small black circles) in the unreconstructed phase (1 × 1) for x = 0.25 and the reconstructed phases c(2 × 2) for x = 0.15 and (2 × 2) for x = 0.05. The red arrows are the unit cell basis vectors; for x = 0.15 the basis vectors (broken arrows) of the rectangular (2 × 1) cell are also shown. The white circles indicate inequivalent atoms in the reconstructed phases, independently of being Mo or Re (which randomly substitutes Mo in its bcc lattice). The parallel rows of atoms linked by H bridges in the [001] direction are associated with a quasi-1D free-electron gas. (b) The cubic symmetry directions of the bcc(110) surface, and (c) the corresponding symmetry points in two adjacent Brillouin zones for the unreconstructed phase.

exhibits a sharp minimum (originally understood as a giant Kohn anomaly). As discussed below in Section 3.2, the finite energy of the minimum indicates the opening of a gap associated with the formation, below a critical temperature, of a charge density wave (CDW) in the $\bar{\Gamma}\bar{H}$ direction, of which the small peaks observed in Figure 3b are the diffractive signature.

At a larger Re concentration x = 0.15, there are weak peaks in the $\bar{\Gamma}\bar{N}$ direction (Figure 4b) corresponding to the zone boundary points N (cfr. Figure 1c), whereas no diffraction peak at all is detected in the $\bar{\Gamma}\bar{S}$ direction (Figure 4a), apart from some weak features which can hardly be related to any diffraction. The Rayleigh wave (RW) dispersion curves of the H-saturated surface with x = 0.15, measured with HAS and presented below in Section 3.2, show, however, folding points at N/2 in the $\bar{\Gamma}\bar{N}$ and $\bar{\Gamma}\bar{H}$ directions, but not at S/2 in the $\bar{\Gamma}\bar{S}$ direction, which tells that a c(2 × 2) reconstruction (Figure 1a), with a (2 × 1) unit cell, does occur and is preserved beneath the H-saturated surface, at a depth compatible with the RW penetration depth. Finally, for x = 0.25 (Figure 4c) only Γ diffraction peaks are observed, which confirms the (1 × 1) structure.

LEED measurements by Okada et al.[25] would suggest that a hydrogen monolayer coverage removes reconstruction, yielding a (1 × 1) surface structure for H/$Mo_{1-x}Re_x$(110) at all concentrations $0 \le x \le 0.25$.[25] A similar conclusion would be drawn from HAS diffraction spectra shown in panels (a) and (b) of Figure 2, measured for x = 0.05, at the same He beam incident energy E_i = 36.9 meV in the $\bar{\Gamma}\bar{S}$ direction, but at a larger E_i = 70.6 meV (Figure 2c), and therefore at a deeper

https://doi.org/10.1021/acs.jpcc.5c04084
J. Phys. Chem. C 2025, 129, 17632−17642

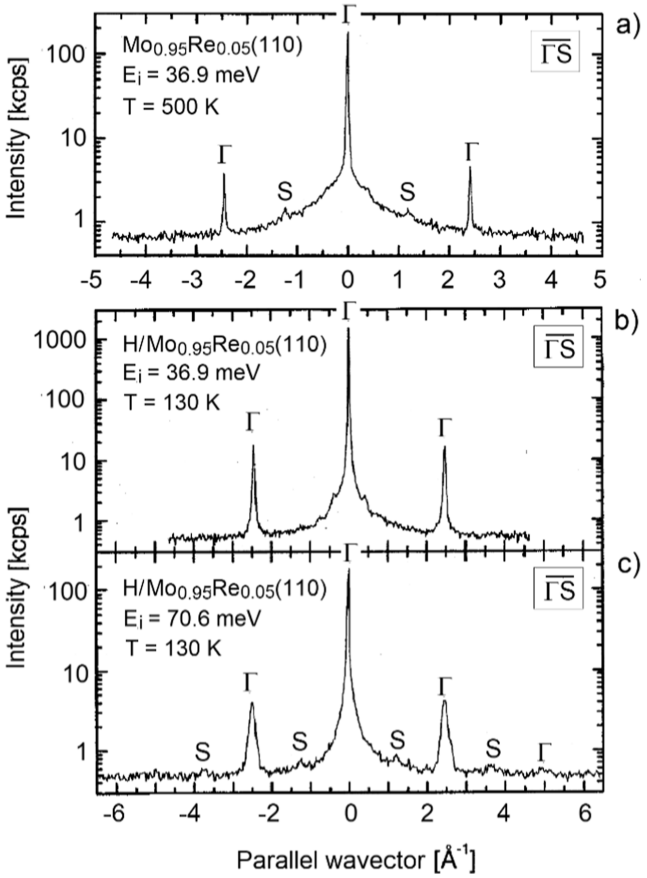

Figure 2. HAS diffraction spectrum of (a) the clean $Mo_{0.95}Re_{0.05}(110)$ surface at 500 K measured as a function of the parallel wavevector transfer with an incident energy of 36.9 meV in the $\overline{\Gamma}\overline{S}$ direction, showing, in addition to the Γ peaks of the unreconstructed phase, the small S peaks signaling a weak (2 × 2) reconstruction. The H-monolayer coverage (b) at 130 K apparently hides the substrate reconstruction, which (c) is however observed at a larger HAS incident energy of 70.6 meV, due to the larger penetration of the scattering He atoms into the surface charge density.

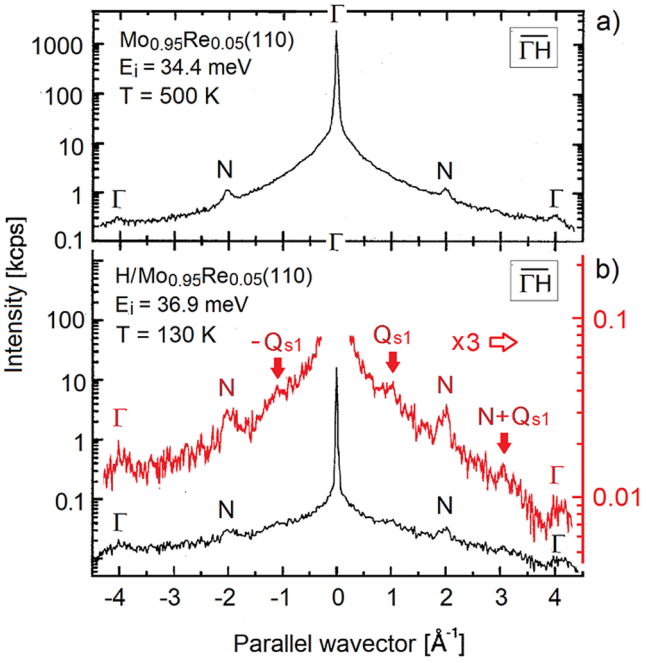

Figure 3. HAS diffraction spectrum of the clean (a) and the H-covered (b) $Mo_{0.95}Re_{0.05}(110)$ surface at the respective surface temperature of 500 and 130 K, and incident energy of 34.4 and 39.6 meV, in the $\overline{\Gamma}\overline{N}$ direction. In this case the small diffraction peaks N are observed for the H-covered surface also at the low incident energy of 36.9 meV, which confirms the (2 × 2) reconstruction. A factor 3 magnification of the spectrum (red line, symbols and right-hand ordinate scale) reveals small features at the wavevectors $\pm Q_{s1} \cong \pm 1$ $Å^{-1}$ and N + Q_{s1}, which are interpreted as the signatures of a charge density wave in the $\overline{\Gamma}\overline{H}$ direction.

penetration into the surface charge density, the S peaks are still there. Moreover, in the $\overline{\Gamma}\overline{N}$ direction (Figure 3) the N peaks are observed with a H-monolayer coverage also at the same incident energy of 36.9 meV, which confirms that the (2 × 2) surface reconstruction is intrinsic to the alloy and survives beneath the H monolayer. In the following derivation of the EP interaction, the (1 × 1) surface unit cell area shall be used for Mo(110) (a_c = 7.06 $Å^2$, from a lattice constant a_0 = 3.15 Å[26]), while for the (1 × 1) surface unit cell of $Mo_{0.75}Re_{0.25}$ (110) (a_c = 6.75 $Å^2$, from a lattice constant of a_0 = 3.09 Å), the (2 × 2) surface unit cell of $Mo_{0.95}Re_{0.05}$ (110) (a_c = 4 × 7.01 $Å^2$ = 28.04 $Å^2$), and the (2 × 1) surface unit cell of $Mo_{0.85}Re_{0.15}$ (110) (a_c = 2 × 6.88 $Å^2$ = 13.76 $Å^2$), the HAS diffraction data of Figures 3−5 are used.[10] The experimental uncertainty of these HAS diffraction spectra does not allow to appreciate the expected contraction of the surface lattice parameter of the H-covered surfaces, measured at 130 K, with respect to that of the clean surfaces, measured at 500 K. This is justified by the small value of the linear thermal expansion coefficient (LTEC) of Mo (4.8 × 10^{-6} K^{-1}),[27] which would give for a cooling from 500 to 130 K just a −0.22% contraction of the unit cell area. This small correction will be applied to the above surface unit cells in the following derivations of the EP coupling for the H-covered alloy surfaces.

3. RESULTS AND DISCUSSION

3.1. Electron−Phonon Interaction from Elastic HAS.

The available HAS data on the H-covered $Mo_{1-x}Re_x(110)$ permit to extract the surface electron−phonon interaction (mass-enhancement factor λ_{HAS}) for x = 0.05 and 0.25 from the dependence on the He-atom incident energy E_i of the specular scattering intensity $I(E_i)$, while the value of λ_{HAS} for x = 0.15 is obtained from the comparison of its diffuse elastic scattering intensity with that for x = 0.25 at the same incident energy and incident angle, away from the specular direction. In the first case, the mass-enhancement factor λ_{HAS} is given by the equation[28]

$$\lambda_{HAS} = \frac{\pi\phi}{2n_s a_c k_B T}\left|\frac{\Delta \ln I(E_i)/k_i}{\Delta {k_{iz}}^2}\right| \quad (1)$$

where $k_i = \sqrt{2mE_i}/\hbar$ is the incident wavevector, m the He atom mass, k_{iz} the component of $\mathbf{k}_i$ normal to the surface, T the surface temperature, a_c the area of the surface unit cell, and ϕ the surface work function. Measurements by Berge et al.[29] for the clean Mo(110) annealed at ∼920 K give ϕ = 4.95 + 0.02 eV, while the exposure of Mo(110) to hydrogen above 0.5 ML was reported by Ernst-Vidalis and Bauer[30] to slowly increase ϕ up to about ∼0.13 eV at 1 ML, which means ϕ = 5.08 eV for H/Mo(110). Since the thermionic work function for the low-index surfaces of rhenium are reported[31] in the same range of

https://doi.org/10.1021/acs.jpcc.5c04084
J. Phys. Chem. C 2025, 129, 17632−17642

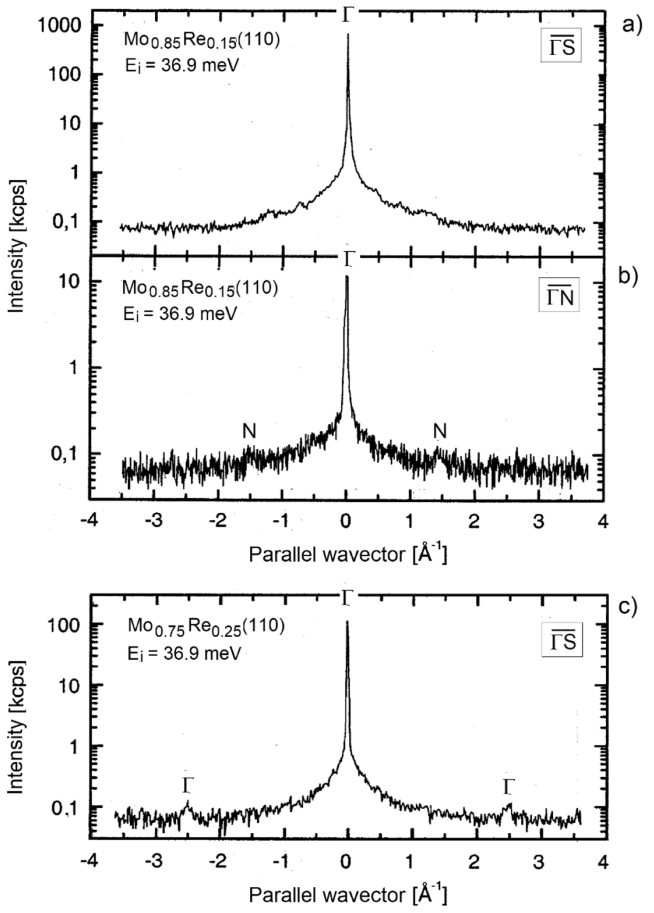

Figure 4. HAS diffraction spectra from the clean $Mo_{0.85}Re_{0.15}(110)$ surface at 500 K in the $\bar{\Gamma}\bar{S}$ (panel (a)) and $\bar{\Gamma}\bar{N}$ (panel (b)) directions; the symmetric pair of weak diffraction peaks N along $\bar{\Gamma}\bar{N}$ can be associated with the c(2 × 2) reconstruction, while the Γ peaks expected at about ±2.8 $Å^{-1}$ are not resolved from the noise. For the unreconstructed clean $Mo_{0.75}Re_{0.25}(110)$ surface (panel (c)) only the Γ peaks are detected.

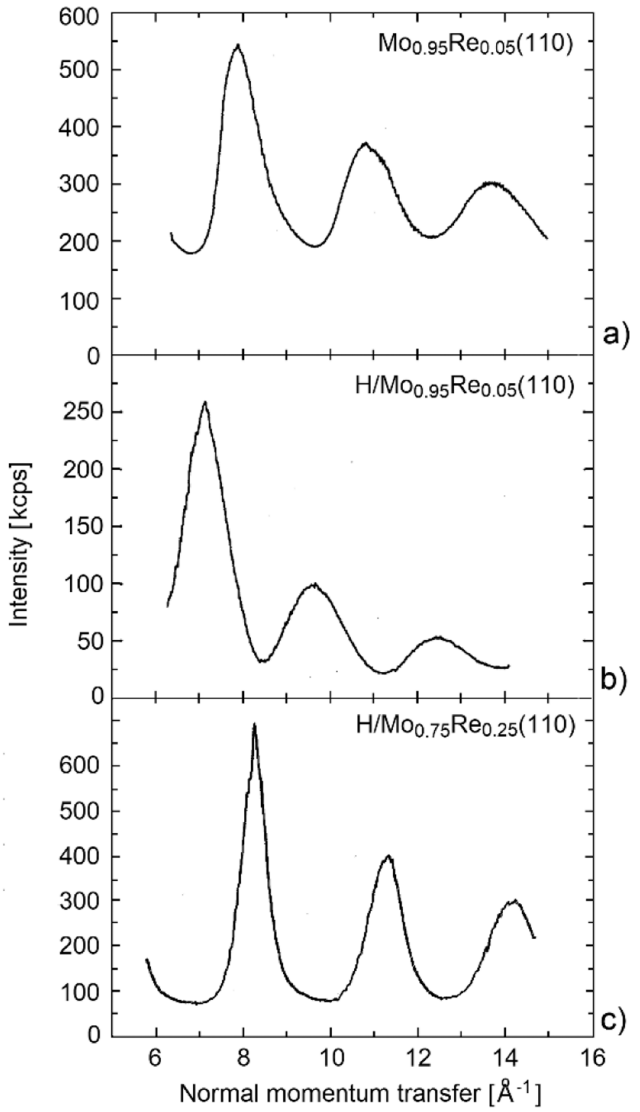

Figure 5. HAS drift spectra[10] showing the interference as a function of the normal momentum transfer between specular peaks reflected from above and below a surface step parallel to [001] for: (a) the clean surface at 500 K and (b) the hydrogen-covered $Mo_{0.95}Re_{0.05}(110)$ surface at 130 K, and for (c) the hydrogen-covered $Mo_{0.75}Re_{0.25}(110)$ surface, also at 130 K. The maxima, corresponding to in-phase interference, are equivalent to the specular intensity in the absence of steps.

4.86−4.96 eV, the same values of ϕ = 4.95 and 5.08 eV could be adopted also for the clean and the H-covered surfaces of the three alloys, respectively. However, the work function also depends on the surface temperature. This correction can be estimated from the work function temperature coefficient of Mo reported by Comsa et al.,[32] $d\phi/dT = (7.84 \pm 0.07)10^{-5}$ eV/K. This gives, for a temperature decrease of (500 −130) K = 370 K, a change of ϕ of −0.6%; thus, ϕ = 5.05 eV shall be used for the H-covered surfaces.

The parameter n_s, representing the effective number of atomic layers contributing to the surface EP interaction, actually reflects the multiplicity of surface electronic bands and their Fermi contours at the Fermi energy. As seen in density-functional calculations (DFT) by Kohler et al.[33] and by Yakovkin et al.[34] for the clean and H-covered Mo(110) surfaces, there are, within one surface Brillouin zone of the clean surface, two complete (four half) Fermi contours around the symmetry point S, one complete (two half) contours around N, and two complete contours around Γ, which makes altogether five. Similarly, for the H-covered surfaces, besides the contours surrounding S and N points, there are two small elliptical contours in the ΓH direction (sections of two downward conic bands, see Figure 3 (right) of ref 34). Thus, n_s = 5 shall be adopted in all the following estimations of λ_{HAS}, also for the clean and H-covered $Mo_{1-x}Re_x(110)$ alloy surfaces. The difference in temperatures, which clean and H-covered surfaces refer to, should not affect the topology of the Fermi contours, nor n_s.

With these input data, the two values of the HAS specular intensity from $H/Mo_{0.95}Re_{0.05}(110)$, as given in Figure 2b,c for two different incident energies of 36.9 and 70.6 meV, give from eq 1 λ_{HAS} = 0.44. A consistent value is found from the dependence on the incident energy of the specular intensity at the maxima of HAS drift spectra (Figure 5b).[10] Drift spectra consist of oscillations of the HAS specular intensity, observed when scattering occurs at a surface step, as a consequence of interference between beams scattered above and below the step. The peak separation permits to determine the step height, but what is important here is the fact that maxima correspond to in-phase scattering, as from an ideal surface, and the

https://doi.org/10.1021/acs.jpcc.5c04084
J. Phys. Chem. C 2025, 129, 17632−17642

dependence of their intensities on the incident normal momentum transfer can be used to determine λ_{HAS}. The three different intensity ratios between the three peak intensities give, from eq 1, $\lambda_{HAS} = 0.43 \pm 0.07$ at the experimental temperature of 130 K. For comparison, the drift spectrum for the clean $Mo_{0.95}Re_{0.05}(110)$ (Figure 5a),[10] measured at 500 K, gives $\lambda_{HAS} = 0.34 \pm 0.05$.

A drift spectrum has been also measured for H/$Mo_{0.75}Re_{0.25}(110)$ at 130 K (Figure 5c), which also permits to extract with eq 1 a mass-enhancement factor $\lambda_{HAS} = 0.78 \pm 0.12$. This shows that the increase of Re concentration produces a considerable increase of λ_{HAS}. A similar effect has been reported by Tulina and Zaitsev[35] from point-contact spectroscopy measurements of quasi-local vibrations in $Mo_{1-x}Re_x$ alloys for $0 \le x \le 0.2$. The values obtained from a linear interpolation of their data are $\lambda = 0.48$ for $x = 0.05$ and $\lambda = 0.76$ for $x = 0.25$, thus showing an increase with Re concentration, very similar in percent to that found with HAS for the corresponding H-covered alloy surfaces.

For H/$Mo_{0.85}Re_{0.15}(110)$, as well as for the clean $Mo_{0.85}Re_{0.15}(110)$ surface, no reliable drift measurements could be done, paradoxically due to the excellent quality of the surface, with an exceedingly low surface step density (surface step-free areas of the order of 10^5 Å^2).[10] This gave, however, the opportunity to devise another method to extract the ME factor from HAS measurements. It consists in extracting the ME factor λ_{HAS} from the comparison of the diffuse elastic (DE) scattering intensities to those of H/$Mo_{0.75}Re_{0.25}(110)$ measured at the same incident angle ($\theta_i = 48°$), incident energy ($E_i = 36.9$ meV), surface temperature (130 K) and scattering plane direction $\overline{\Gamma}\overline{S}$ (Figure 6). The diffuse elastic (DE) intensity originates mostly from the thermal disorder at the surface, and takes therefore the form $I(x) = I_0 \exp[-2W(x)]$, where the prefactor I_0 under the above conditions is independent of x, while the DW exponent[28]

$$2W(x) = \frac{n_s a_c(x)(\Delta \mathbf{k})^2}{2\pi\phi} k_B T \lambda_{HAS}(x) \tag{2}$$

only depends on x, within the present approximations, through the surface unit-cell area and the mass-enhancement factor. In eq 2

$$(\Delta \mathbf{k})^2 = k_i^2[(\cos\theta_i + \cos\theta_f)^2 + (\sin\theta_i - \sin\theta_f)^2] \tag{3}$$

where $\theta_f = 101.7° - \theta_i$ is the final angle.[28] For incidence close to the specular condition the second term, accounting for the parallel momentum transfer, can be neglected. Thus, with the help of eq 1, one has that

$$a_c(0.25)\lambda_{HAS}(0.25) - a_c(0.15)\lambda_{HAS}(0.15) = \frac{\pi\phi}{2n_s k_{iz}^2 k_B T} \ln \frac{I(0.15)}{I(0.25)} \tag{4}$$

With the DE intensity values from Figure 6, the input data, the value $\lambda_{HAS}(0.25) = 0.78 \pm 0.12$ for H/$Mo_{0.75}Re_{0.25}(110)$ and the ratio $a_c(0.15)/a_c(0.25) = 2$ discussed above, one obtains for H/$Mo_{0.85}Re_{0.15}(110)$, $\lambda_{HAS}(0.15) = 0.58 \pm 0.09$. This value compares well, within the experimental error, with the value $\lambda = 0.64$ interpolated from the Tulina and Zaitsev results.[35]

The DE peak intensity, when available as a function of the surface temperature at constant scattering geometry and incident energy, may also be used to extract λ_{HAS}. An example is illustrated in Figure 7 on the basis of a few available HAS-

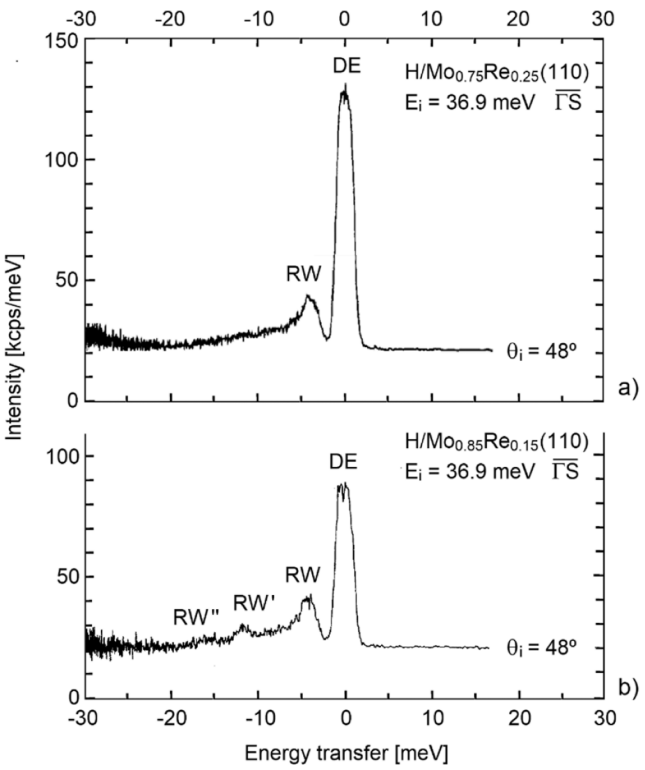

Figure 6. Time-of-flight (TOF) HAS spectra (plotted as functions of the energy transfer) measured with an incident energy of 36.9 meV and an incident angle $\theta_i = 48°$, close to specular condition ($\theta_i = 50.85°$, with a fixed scattering angle of 101.7°) in the $\overline{\Gamma}\overline{S}$ direction, for the H-covered $Mo_{0.75}Re_{0.25}(110)$ (panel (a)) and $Mo_{0.85}Re_{0.15}(110)$ (panel (b)) surfaces at 130 K. The comparison between the intensities of the diffuse elastic peaks DE, as well as between the inelastic intensities associated with the creation of Rayleigh waves (RW, RW′, RW″, see Figure 8 below) is used to extract information on the EP interaction for $x = 0.15$.

TOF data for the clean Mo(110) measured by Lüdecke.[6] Above 120 K and up to 500 K the DE peak intensity shows the expected attenuation due to the DW factor (see in ref 36 Figures 7 and 10b), while a jump to a larger value above 600 K may be attributed to a setup of some surface disorder. The slope of the DE intensity on a logarithmic scale, i.e., the DW exponent, in the range 120−500 K (Figure 7b) provides λ_{HAS} for Mo(110) from eq 2, with $n_s = 5$, $a_c(0) = 7.06$ Å^2, $\phi = 4.95$ eV, $k_i = 8.6$ Å^{-1}, and $(\Delta \mathbf{k})^2 = 118$ Å^{-2}. This gives $\lambda_{HAS} = 0.37$ with an estimated uncertainty of ±0.05.

The values of λ_{HAS} obtained above are listed in column 2 of Table 1 and compared with the values of λ for the clean surfaces interpolated from those reported by Tulina and Zaitsev[35] for other values of x, as well as with those more recently obtained by Shang et al.[17] The superconducting critical temperature T_c, listed in column 7 of Table 1, has been calculated from these values of λ_{HAS} with the McMillan formula[4,37]

$$T_c = \frac{\theta_D}{1.45} \exp\left[\frac{-1.04(1 + \lambda_{HAS})}{\lambda_{HAS} - \mu^*(1 + 0.62\lambda_{HAS})}\right] \tag{5}$$

where the effective Coulomb repulsion μ^* has been set equal to 0.1 for all surfaces, as suggested by Grimwall,[38] and θ_D is the Debye temperature of the sample. The latter is assumed to depend on Re concentration according to the equation

https://doi.org/10.1021/acs.jpcc.5c04084
J. Phys. Chem. C 2025, 129, 17632−17642

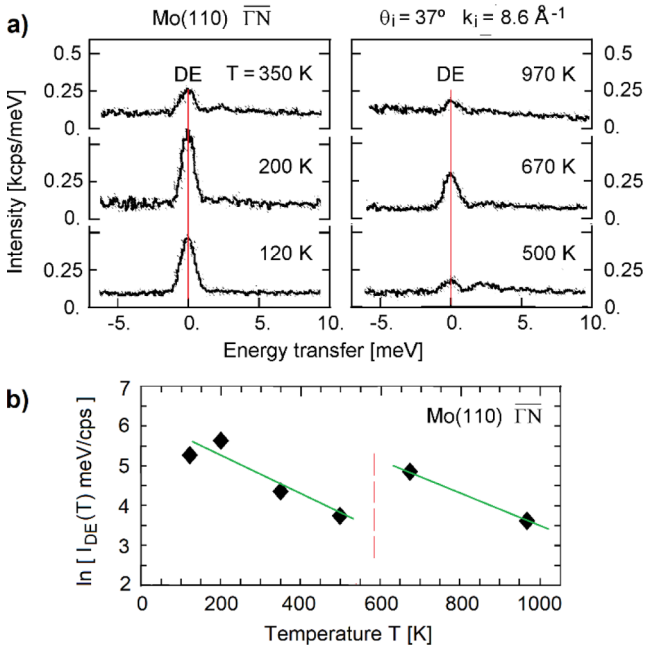

Figure 7. (a) HAS-TOF spectra (from Lüdecke[6]) for the clean Mo(110) surface in the [1$\bar{1}$0] ($\bar{\Gamma}\bar{N}$) direction showing the diffuse elastic (DE) peak at different surface temperatures at a constant incident angle of 37° (scattering angle: 101.7°) and momentum of 8.6 Å^{-1}. (b) Plot of DE intensity on a logarithmic scale as a function of temperature (♦) showing the slopes (green straight lines) of the DW exponent below and above a possible transition to some surface disorder above about 600 K.

$$\theta_D(x) \cong \theta_D(0)\sqrt{\frac{M_{Mo}}{(1-x)M_{Mo} + xM_{Re}}} \quad (6)$$

where M_{Mo} = 95.9 and M_{Re} = 186.2 are the atomic masses of Mo and Re, respectively.

This approximation is justified by the fact that the Debye temperatures of Mo and Re, $\theta_D(0)$ = 377 K and $\theta_D(1)$ = 275 K,[39] scale almost exactly as the inverse square root of the masses, thus indicating almost identical effective interatomic force constants f of the two metals: $f_{Re}/f_{Mo} = [\theta_D(1)/\theta_D(0)]^2$ M_{Re}/M_{Mo} = 1.03. The values of θ_D for the H-covered surfaces are approximated to those for the clean surfaces obtained from eq 6. They are listed in Table 1, columns 5 and 6, together with the values of θ_D adopted by Shang et al.[17] in their derivation of λ from the experimental T_c (last column) for the alloy clean surfaces. In that derivation, Shang et al. used μ^* = 0.13; the T_c values for the H-covered surfaces calculated from λ_{HAS} with μ^* = 0.1 but Shang et al. values of θ_D are also given in the last column for comparison (in parentheses).

3.2. Electron−Phonon Interaction from Inelastic HAS.

The TOF spectra in Figure 6 also show the inelastic peaks associated with the creation of a Rayleigh wave in the backward (RW) and forward (RW′, RW″) directions. The kinematics is illustrated in Figure 8 showing the scan curve (red curve) (see ref 36 Chapter 9) for the incident angle θ_i = 48°, incident energy E_i = 36.9 meV and scattering angle of 107.7°. The observed inelastic peaks correspond to the intersections (red circles) of the scan curve with the RW dispersion curves (green for x = 0.15, black for x = 0.25), interpolating the experimental HAS points (green squares for x = 0.15, gray lozenges for x = 0.25) associated with the RW and reproduced in both positive and negative $\bar{\Gamma}\bar{S}$ directions. An arrow indicates the experimental RW frequency at $\bar{S}$ also for x = 0.05 (for the full set of data see ref 10). While at long wavelengths the RW is observed at about the same energy independently of x, the RW′ and RW″ peaks are only observed for x = 0.15 (and 0.05), and not for x = 0.25 due to the large softening of the RW phonons at short wavelengths for the largest Re concentration.

Since the RW penetration into the bulk is proportional to the wavelength, the softening induced by Re is produced by some important change occurring in the surface region. Although Re has an atomic mass which is almost twice that of Mo with a slightly smaller atomic size, a Re segregation in the surface region with increasing concentration does not seem to be sufficient to explain such a large softening of short-wave Rayleigh phonons. An additional contribution from the

Table 1. Electron-Phonon Interaction (Mass-Enhancement Factor λ) from HAS Data (λ_{HAS}) for the (110) Surfaces of Clean and H-Covered Mo and Mo/Re Alloys Compared with λ for the Clean Surfaces from Other Sources[e,17,35]

		λ clean surface		θ_D [K]		T_c [K] experiment	
surface	λ_{HAS}	[35][a]	[17][b]	eq 6	[17][b]	HAS	[17][d]
Mo(110)	0.37 ± 0.05	0.39	0.41	377	460.0	0.81	0.92
H/Mo(110)	0.38 ± 0.06[c]	-	-	377	-	0.96	(1.18)
$Mo_{0.95}Re_{0.05}$(110)	0.34 ± 0.05	0.48	0.46	368	445.0	0.44	1.97
H/$Mo_{0.95}Re_{0.05}$(110)	0.43 ± 0.07	-	-	368	-	1.89	(2.28)
$Mo_{0.85}Re_{0.15}$(110)	-	0.64	0.62	-	436.2	-	6.54
H/$Mo_{0.85}Re_{0.15}$(110)	0.58 ± 0.09	-	-	353	-	6.02	(7.43)
$Mo_{0.75}Re_{0.25}$(110)	-	0.76	0.69	-	480.6	-	10.32
H/$Mo_{0.75}Re_{0.25}$(110)	0.78 ± 0.12	-	-	339	-	12.5	(17.68)

[a]Values for the clean surfaces interpolated from those reported by Tulina and Zaitsev[35] for other values of Re concentration x. [b]Values of θ_D from Shang et al.[17] The value for x = 0.05 is linearly interpolated between those reported by these authors for x = 0 and x = 0.10. [c]Extrapolated from the values for the H-covered samples with x > 0. [d]T_c for the clean surfaces from Shang et al.[17] In parentheses T_c calculated with eq 5 for the H-covered surfaces from λ_{HAS} with μ^* = 0.1 and θ_D from Shang et al.[17] (6th column). [e]The corresponding critical superconducting temperature T_c, derived with the McMillan formula[4,37] from λ_{HAS} and the Debye temperature θ_D (columns 5 and 6), is given in the last two columns and compared with Shang et al. experimental T_c for the corresponding clean surfaces.[17]

https://doi.org/10.1021/acs.jpcc.5c04084
J. Phys. Chem. C 2025, 129, 17632−17642

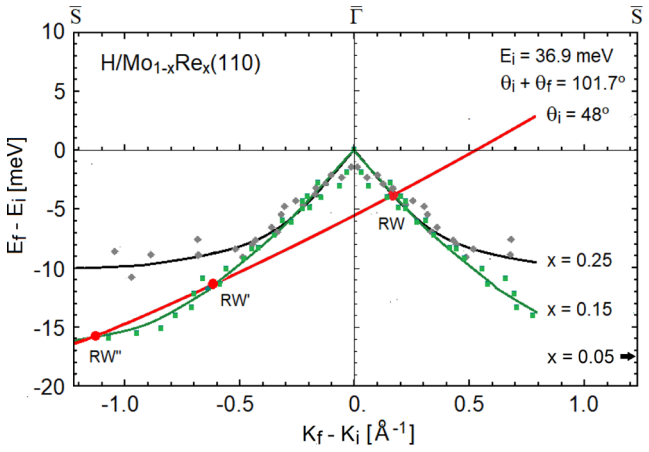

Figure 8. Rayleigh wave (RW) dispersion curves of H/$Mo_{1-x}Re_x$(110) measured in the $\bar{\Gamma}\bar{S}$ direction with HAS at a surface temperature of 130 K for x = 0.15 (gray lozenges) and 0.25 (green squares). For x = 0.05 only the zone-boundary value at $\bar{S}$ is indicated by an arrow. At short wavelengths, when the RW penetration depth is restricted to just a few layers, a dramatic softening is observed with the increase of Re concentration and corresponding increase of λ_{HAS}. Thus, the HAS scan curve (red curve) for the two spectra of Figure 6 intersects the RW for x = 0.15 at three points (RW, RW′, RW″), while only the RW backward creation process is observed for x = 0.25.

increased EP interaction at the larger Re concentrations in H-covered samples is expected.

Density-functional perturbation theory (DFPT) calculations by Sklyadneva et al.[40] showed that the inelastic HAS amplitudes from superconducting Pb films grown on Cu(111)[41] are proportional to the mode-selected EP coupling constants for each individual phonon. Since in the power expansion of exp[−2W], unitarity implies that single-phonon processes are weighed by the factor W exp[−2W], and the HAS inelastic intensities $I_{RW}(x)$ for the same RW phonon in panels (a) (x = 0.25) and (b) (x = 0.15) of Figure 6, having the same weight in the total phonon spectrum, are proportional to this factor. Thus, from eq 2, this implies

$$\frac{\ln[I_{RW}(0.15)/I(0.15)]}{\ln[I_{RW}(0.25)/I(0.25)]} = \frac{W(0.15)}{W(0.25)} = \frac{a_c(0.15)\lambda_{HAS}(0.15)}{a_c(0.25)\lambda_{HAS}(0.25)} = 2\frac{\lambda_{HAS}(0.15)}{\lambda_{HAS}(0.25)} \quad (7)$$

where, as above, $I(x)$ is the intensity of the DE peak. With the intensity ratios from Figure 6 one obtains λ_{HAS} (0.15)/λ_{HAS} (0.25) = 0.738, which is almost identical to the ratio 0.750 found above from the ratio of the DE peaks. This shows that also the inelastic HAS intensities are suitable to extract information on λ_{HAS}, albeit through a comparison procedure.

The dependence of the ME factor λ_{HAS} (x) on the Re concentration x as obtained from HAS measurements is shown in Figure 9 (full and open lozenges for H-covered and clean alloy surfaces, respectively). The good linearity of λ_{HAS} (x) (full straight line) permits to extrapolate the value of λ_{HAS} (0) = 0.38 for H/Mo(110), slightly above that for the clean surface. For x = 0.05 the increase of λ_{HAS} from the clean to the H-covered surface, is more pronounced, although at this stage it cannot be said whether this is a genuine effect of hydrogen or of the large temperature difference. A similar linear growth of the ME factor λ with the Re concentration x is observed for the low-temperature clean-surface data by Shang et al.[17] The two

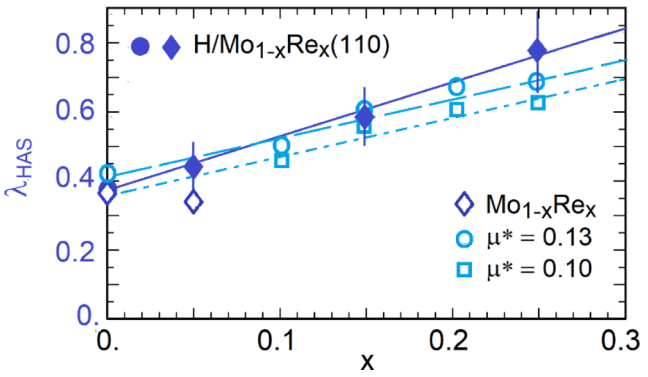

Figure 9. Mass-enhancement factor λ_{HAS} of hydrogen-covered H/$Mo_{1-x}Re_x$(110) alloy surfaces at 130 K from HAS measurements (full lozenges) and its linear fit (full line), providing the extrapolation for H/Mo(110) (x = 0, full circles), are compared to λ_{HAS} for the clean surfaces at 500 K (open lozenges) and to the ME factor of the $Mo_{1-x}Re_x$ alloys derived by Shang et al.[17] from the superconducting T_c via eq 5, with the values of θ_D at 0 K and the Coulomb pseudopotential μ^* = 0.13 (○, fitted by a broken straight line) or μ^* = 0.10, as chosen in the present work (□, linearly fitted by a dash-dotted line).

plots in Figure 9 show $\lambda(x)$ derived from the experimental superconducting T_c, with the Debye temperature θ_D at 0 K and the Coulomb pseudopotential μ^* equal to either 0.13, as chosen by Shang et al. for transition metals (○ in Figure 9, fitted by a broken straight line), or μ^* = 0.10, as chosen in the present work (□ in Figure 9, fitted by a dash-dotted straight line). It appears that H-coverage yields a faster growth of λ_{HAS} with the Re concentration (at 130 K) than that derived for clean alloy surfaces at low temperature, thus an increase of the ME factor induced by hydrogen adsorption which becomes more pronounced with increasing Re concentration.

The most intriguing manifestation of the EP interaction associated with H- coverage which has been discovered with HAS is, however, the so-called giant (and very sharp) Kohn anomaly,[6−11] which has been observed to occur in the RW dispersion curves of all H-covered $Mo_{1-x}Re_x$ samples at certain wavevectors Q_{s1} (indicated by red arrows in Figure 10), but not for clean surfaces.[7−10] This anomaly is also observed in the $\bar{\Gamma}\bar{S}$ direction at a wavevector Q_{s2} near the zone boundary.

As discussed by Kohler et al.[42] on the basis of first-principle calculations, the giant anomaly is actually the edge dispersion curve of the electron−hole (e−h) excitation spectrum of a quasi-one-dimensional free electron gas, associated with a good nesting at the Fermi contours induced by the adsorbed H monolayer. The nesting wavevectors measured for H/Mo(110) along $\bar{\Gamma}\bar{N}$ (Figure 10c, Q_{s1} = 0.89 Å^{-1}), as well as along $\bar{\Gamma}\bar{S}$ at Q_{s2} = 1.22 Å^{-1},[10] are indeed in close agreement with DFT calculations (0.86 Å^{-1} and 1.23 Å^{-1}, respectively[33]). The electronic nature of the giant anomaly also explains why it is not observed by EELS,[43] except for the phonon-like segments in the avoided-crossing region of the RW and e-h excitation dispersion curves (see section 11.3.6 in ref 36). Such segments, assigned to a weak Kohn anomaly, yield for H/Mo(110) a value of λ as small as 0.11 ± 0.02.[44,45] The EP interaction, besides causing the above avoided crossing, is reflected in the fact that the energy of the giant anomaly does not reach zero at Q_{s1} for any value of Re concentration x, but has a minimum (red mark on the left ordinate scales in Figure 10c−f), which increases with x and the corresponding λ_{HAS}.

https://doi.org/10.1021/acs.jpcc.5c04084
J. Phys. Chem. C 2025, 129, 17632−17642

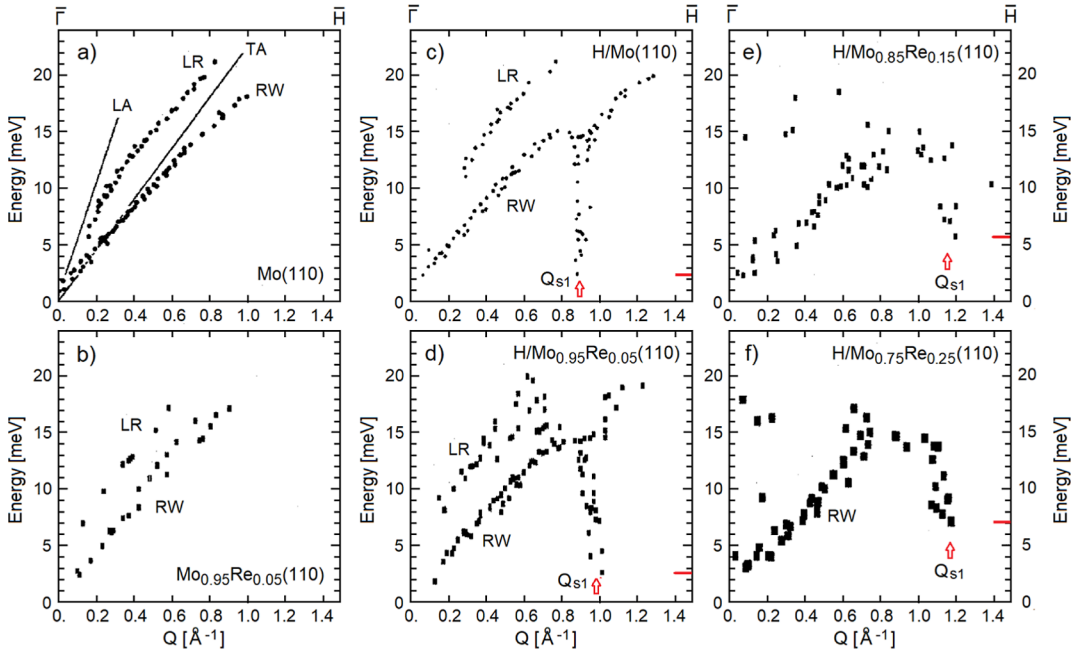

Figure 10. (a) The HAS dispersion curves in the $\bar{\Gamma}\bar{H}$ direction of the RW and of the longitudinal acoustic resonance (LR) (dots), compared with the bulk transverse (TA) and longitudinal (LA) acoustic phonon slopes in the long-wave limit (straight lines) for the clean Mo(110),[10] and (b) $Mo_{0.95}Re_{0.05}$(110) surfaces.[10] (c–f) The hydrogen monolayer coverage induces, at the experimental temperature of 130 K, a giant Kohn anomaly for pure Mo (c), as well as for the alloys with Re percentage of 5% (d), 15% (e), and 25% (f).[10] A red arrow marks the anomaly wavevector $Q = Q_{s1}$. The giant and sharp anomaly actually is the dispersion of electron–hole excitations across the Fermi level of a quasi-1D free-electron gas,[33] where $Q_{s1} = 2k_F$ and k_F the Fermi wavevector. A charge-density wave (CDW) Peierls instability for $T < T_c$ (here above 130 K) opens a gap at Q_{s1} (red horizontal bars marking the anomaly minima).

This is attributed to a Peierls transition leading to the formation of a charge density wave (CDW), with the opening of a gap Δ_{CDW}, equal to the anomaly energy minimum and a T_c which should be well above the experimental temperature of 130 K. The observed anomaly minimum energy, measuring the CDW gap $\Delta_{CDW}(x)$, and the corresponding wavevector $Q_{s1}(x)$ are plotted in Figure 11 (red bars) for the different Re

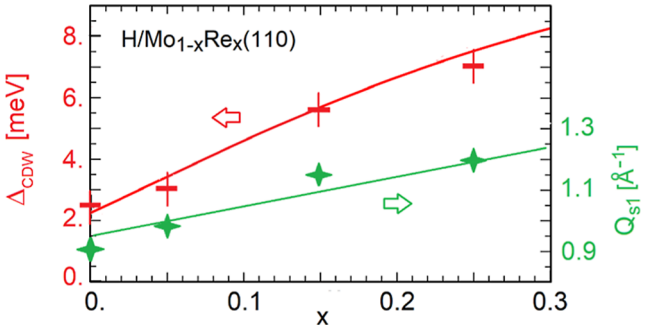

Figure 11. Plots of the minima of the hole–electron dispersion curves, giving the CDW gap $\Delta_{CDW}(x)$ (red bars, left ordinate scale), and of the corresponding wavevectors $Q_{s1}(x)$ (green stars, right ordinate scale) as measured by HAS for the H-covered alloys with x = 0, 0.05, 0.15., and 0.25 (Figure 9). The fitting lines are respectively given by eqs 7 and 8.

concentrations x. $\Delta_{CDW}(x)$ is well represented by an Eliashberg-like gap equation in the BCS limit at 0 K (red curve)[38]

$$\Delta_{CDW}(x) = 2\tau k_B \theta_D(x) e^{-1/\lambda_{HAS}(x)} \quad (8)$$

with $\theta_D(x)$ given by eq 6, and $\lambda_{HAS}(x)$ given by the linear interpolation of the three H-covered alloy values (Figure 9). The factor $\tau = (1 - T/T_c)^{1/2}$, with T_c the CDW transition temperature, accounts for the gap at a finite temperature in the mean-field approximation. The fit in Figure 11 for T = 130 K is obtained with T_c = 173 K. It should be noted, however, that T_c is also dependent on x, but the present limited data do not permit a more accurate fit.

For $H/Mo_{0.95}Re_{0.05}$ a signature of this CDW may be found in the weak diffraction peaks at Q_{s1} and N + Q_{s1} detected in the $\bar{\Gamma}\bar{N}$ direction (Figure 3b). The shift of Q_{s1} to larger values for an increase of the Re concentration x can be viewed as a consequence of the extra-electron provided by Re when replacing a Mo atom, and related changes of the Fermi contours and nesting conditions. Assuming that the quasi-1D free electron gas includes ν electrons per surface metal ion from the hydrogen monolayer plus a fraction x contributed by the replacement of Mo with a Re ion, the proportionality holding for a 1D free-electron gas between the Fermi wavevector and free-electron linear density, $k_F(x) = \pi(\nu + x)/2a_0$, yields, for a_0 = 3.15 Å of Mo(110)[26]

$$Q_{s1}(x) = 2k_F(x) \cong (1.0\text{Å}^{-1})(\nu + x) \quad (9)$$

From the experimental minimum wavevector $Q_{s1}(0) \cong 0.89$ $Å^{-1}$ (Figure 10c), it appears that H adsorption contributes ν = 0.89 electrons per surface atom to the 1D electron gas. This gives a reasonable linear fit of the few experimental data in Figure 11, although the latter would rather suggest a slight downward curvature of $Q_{s1}(x)$ at increasing x, like that of $\Delta_{CDW}(x)$, with a possible saturation at larger x.

The finite penetration depth of the RW, proportional and comparable to its wavelength, allows these waves to probe the

https://doi.org/10.1021/acs.jpcc.5c04084
J. Phys. Chem. C 2025, 129, 17632–17642

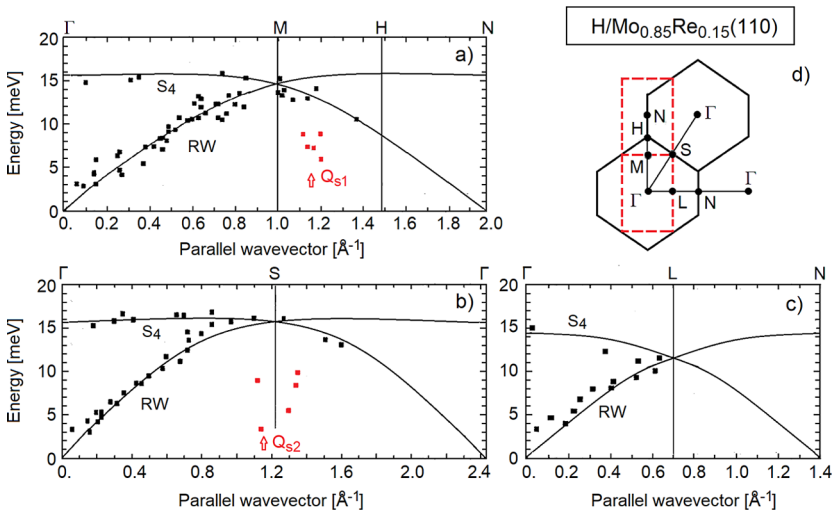

Figure 12. (a,b,c) RW dispersion curves of $H/Mo_{0.85}Re_{0.15}(110)$ measured with HAS (black full squares) along the three symmetry directions depicted in panel (d). The folding points at M, S and N, illustrated by the guidelines representing qualitatively the RW dispersion curves, define in (d) a (2×1) Brillouin zone (dashed red rectangle). The red data points correspond to electron−hole pair excitations responsible for the so-called giant anomalies; the vertical arrows indicate the critical wavevectors Q_{s1} and Q_{s2} as given in ref 10.

structure of the subsurface atomic layers. In particular a subsurface reconstruction with a periodicity doubling in some direction can be signaled by a folding of its dispersion curve. This is the case for $H/Mo_{0.85}Re_{0.15}(110)$ discussed above. Figure 12 shows the HAS data points (black squares) for the RW dispersion curve along the three symmetry directions $\bar{\Gamma}\bar{H}$ (a), $\bar{\Gamma}\bar{S}$ (b) and $\bar{\Gamma}\bar{N}$ (c). The eye guidelines, describing qualitatively the experimental RW dispersion curves show folding points at M along $\bar{\Gamma}\bar{H}$ (a) and L along $\bar{\Gamma}\bar{N}$ (c) that are at the boundaries of the (2×1) Brillouin zone (red broken-line rectangle in (d)). Along $\bar{\Gamma}\bar{S}$ the folding at S, which is also at the zone boundary of the unreconstructed surface, is that of the RW into a surface optical phonon branch (here labeled S_4), as found to occur at the (110) surface of bcc metals, e.g., Fe(110).[46] The observation of the three RW folding points at M, L and S confirms the (2×1) reconstruction of the $H/Mo_{0.85}Re_{0.15}(110)$ surface beneath the hydrogen coverage. Note that for a HAS scattering plane direction not normal to $\bar{\Gamma}\bar{H}$, like the $\bar{\Gamma}\bar{S}$ direction, the giant anomaly, i.e., the quasi-1D electron−hole pair excitations (red squares in Figure 11a,b), keeps being observed at fairly close values of the critical wavevector ($Q_{s1} \cong Q_{s2} \cong 1.14$ Å^{-1}, as given in ref 10). On the other hand, the CDW gap along $\bar{\Gamma}\bar{S}$ appears to be smaller than along $\bar{\Gamma}\bar{H}$, as long as one may judge from the few available experimental points, as expected from a strong anisotropy in the momentum space associated with the quasi-1D structure yielding the giant anomalies.

4. CONCLUSIONS

The HAS method to obtain information on the electron−phonon interaction at conducting surfaces has been applied to the (110) surface of H-covered $Mo_{1-x}Re_x$ alloys, known for the occurrence of a sharp giant anomaly in the dispersion relation of acoustic surface phonons. The mass-enhancement factor λ_{HAS} obtained for H-covered surfaces, is comparable to that of clean surfaces found in the literature at small values of the Re concentration x, but it increases faster with x than that of clean surfaces, so as to exhibit a 23% increase in the H-covered alloy for $x = 0.25$ over the corresponding clean surface. On the other hand, the direct comparison of HAS measurements on both H-covered and clean surfaces, only available for $x = 0.05$, indicates a 30% increase already at such a small RE concentration. Although conspicuous, this would not be enough the explain the sharp and profound dips observed in the phonon dispersion curves of H-covered samples as ordinary Kohn anomalies induced by the EP coupling. They are, as already argued in the past, the dispersion curves of electron−hole excitations in the presence of a CDW superstructure, thus confirming that HAS can probe electron−hole excitations and reveal CDW gaps related to the size of the EP interaction.

The present study, in addition to extracting new information from old data, most of which is available in the literature, is also proposing new ways to obtain information on the surface electron−phonon interaction (mass-enhancement factor) from HAS, such as the analysis of the drift spectra, the analysis of the dependence on temperature of DE scattering intensity and the comparison of the DE intensities measured at different compositions of superconducting alloys. Moreover, also inelastic HAS from one-phonon creation processes has been shown to provide information on the EP interaction. Actually, this corroborates the early demonstration by Sklyadneva et al.[20] that the inelastic HAS amplitudes from single surface phonons are proportional to the respective, mode-selected, EP coupling constants (mode-lambdas), by providing a more quantitative information. In the present case of H-covered alloy surfaces, where some structural properties peculiar to an alloy (e.g., surface reconstruction, segregation, etc.) can be partially masked by the overlayer, surface phonons can actually convey subsurface information on the scale of the specific phonon penetration depth. This means that a quantitative analysis of the inelastic HAS amplitudes as outlined in Sub 3.2, can provide new tools to investigate the EP interaction in complex 2D superconductors and CDW systems.

It is hoped that the unique ability of HAS to probe the vibrational and some kind of electronic excitations in the THz domain, as well as their interaction, will stimulate new systematic HAS investigations on presently important issues like the coexistence of superconductivity and CDWs[47,48] and

https://doi.org/10.1021/acs.jpcc.5c04084
J. Phys. Chem. C 2025, 129, 17632−17642

the effects of surface hydrogenation on superconductivity in low dimensional systems.[49]

AUTHOR INFORMATION

Corresponding Author

Salvador Miret-Artés − *Donostia International Physics Center, 20018 Donostia-San Sebastian, Spain; Instituto de Física Fundamental, Consejo Superior de Investigaciones Científicas, 28006 Madrid, Spain;* orcid.org/0000-0002-4056-376X; Email: s.miret@iff.csic.es

Authors

Giorgio Benedek − *Donostia International Physics Center, 20018 Donostia-San Sebastian, Spain; Department of Materials Science, University of Milano-Bicocca, 20125 Milano, Italy*

Björn Flach − *Max-Planck-Institut für Dynamik und Selbstorganisation, 37073 Göttingen, Germany;* Present Address: Erminoldstrasse 75, 81735 Munich, Germany

Joseph R. Manson − *Donostia International Physics Center, 20018 Donostia-San Sebastian, Spain; Department of Physics and Astronomy, Clemson University, Clemson, South Carolina 29634, United States*

J. Peter Toennies − *Max-Planck-Institut für Dynamik und Selbstorganisation, 37073 Göttingen, Germany*

Complete contact information is available at: https://pubs.acs.org/10.1021/acs.jpcc.5c04084

Notes

The authors declare no competing financial interest.

ACKNOWLEDGMENTS

S.M.A. acknowledges support of a grant from the Ministery of Science, Innovation and Universities with ref. PID2023-149406NB-I00.

REFERENCES

(1) Syed, H. M.; Webb, C. J.; Gray, E. M. Hydrogen-modified superconductors: A review. *Prog. Solid State Chem.* **2016**, *44*, 20−34.

(2) Drozdov, A. P.; Kong, P. P.; Minkov, V. S.; Besedin, S. P.; Kuzovnikov, M. A.; Mozaffari, S.; Balicas, L.; Balakirev, F. F.; Graf, D. E.; Prakapenka, V. B.; et al. Superconductivity at 250 K in lanthanum hydride under high pressures. *Nature* **2019**, *569*, 528−531.

(3) Semenok, D. V.; Kruglov, I. A.; Savkin, I. A.; Kvashnin, A. G.; Oganov, A. R. On Distribution of Superconductivity in Metal Hydrides. *Curr. Opin. Solid State Mater. Sci.* **2020**, *24*, 100808.

(4) Allen, P. B.; Dynes, R. C. Transition temperature of strong-coupled superconductors reanalysed. *Phys. Rev. B* **1975**, *12*, 905−922.

(5) He, Y.; Shi, J.-J. Few-Hydrogen High-Tc Superconductivity in $(Be_4)_2H$ Nano-superlattice with Promising Ductility under Ambient Pressure. *Nano Lett.* **2023**, *23*, 8126−8131.

(6) Lüdecke, J. Vergleichende Untersuchung der sauberen und adsorbatbedeckten W(110)- und Mo(110)-Oberfläche mit hochauflösender Helium-Atomstrahlstreuung. Dissertation, Max-Planck-Institut für Strömungsforschung, Göttingen, 1994.

(7) Hulpke, E.; Lüdecke, J. Hydrogen-induced phonon anomaly on the W (110) surface. *Phys. Rev. Lett.* **1992**, *68*, 2846−2849.

(8) Hulpke, E.; Lüdecke, J. The giant surface phonon anomaly on hydrogen saturated W(110) and Mo(110). *Surf. Sci.* **1993**, *287*, 837−841.

(9) Hulpke, E.; Lüdecke, J. Surface phonon anomaly induced by adsorption. *J. Electron Spectrosc. Relat. Phenom.* **1993**, *64*−*65*, 641−649.

(10) Flach, B. Phononenanomalien und Elektron-Phonon-Kopplung an Metalloberflächen und dünnen Schichten. Dissertation, Max-Planck-Institut für Strömungsforschung, Göttingen, 2000.

(11) Okada, M.; Flach, B.; Hulpke, E.; Steinhögl, W.; Plummer, E. W. Shifting the surface Kohn anomaly of H-saturated Mo(110) by alloying the bulk with Re. *Surf. Sci. Lett.* **2002**, *498*, L78−L84.

(12) Gavaler, J. R.; Janocko, M. A.; Jones, C. K. A-15 structure Mo−Re superconductor. *Appl. Phys. Lett.* **1972**, *21*, 179−180.

(13) Gavaler, J. R.; Janocko, M. A.; Jones, C. K.; Timmerhaus, K. D. Superconductivity and Metastability in Alloys of the Mo-Re System. In *Low Temperature Physics-LT 13*; Springer: New York, 1974; pp 558−562.

(14) Sundar, S.; Sharath Chandra, L. S.; Chattopadhyay, M. K.; Roy, S. B. Evidence of multiband superconductivity in the β-phase $Mo_{1-x}Re_x$ alloys. *J. Phys.: Condens. Matter* **2015**, *27*, 045701.

(15) Sundar, S.; Chandra, L. S. S.; Chattopadhyay, M. K.; Pandey, S. K.; Venkateshwarlu, D.; Rawat, R.; Ganesan, V.; Roy, S. B. Strong electron−phonon coupling and multiband effects in the superconducting β-phase Mo_{1-x} Re_x alloys. *New J. Phys.* **2015**, *17*, 053003.

(16) Sundar, S.; Banik, S.; Sharath Chandra, L. S.; Chattopadhyay, M. K.; Ganguli, T.; Lodha, G. S.; Pandey, S. K.; Phase, D. M.; Roy, S. B. Electronic structure of $Mo_{1-x}Re_x$ alloys studied through resonant photoemission spectroscopy. *J. Phys.: Condens. Matter* **2016**, *28*, 315502.

(17) Shang, T.; Gawryluk, D. J.; Verezhak, J. A. T.; Pomjakushina, E.; Shi, M.; Medarde, M.; Mesot, J.; Shiroka, T. Structure and superconductivity in the binary Re $_{1-x}$ Mo_x alloys. *Phys. Rev. Mater.* **2019**, *3*, 024801.

(18) Tarenkov, V.; Shapovalov, A.; Zhitlukhina, E.; Belogolovskii, M.; Seidel, P. Mo-Re alloy: A new benchmark two-band superconductor. *Low Temp. Phys.* **2023**, *49*, 103−107.

(19) Kresin, V. Z.; Ovchinnikov, S. G.; Wolf, S. A. *Superconducting State: Mechanisms and Materials*; Oxford University Press, Oxford, 2021, Chapter 3.2.

(20) Sklyadneva, I. Y.; Benedek, G.; Chulkov, E. V.; Echenique, P. M.; HeidBohnenToennies, R. K. P. J. P.; Bohnen, K.-P.; Toennies, J. P. Mode-Selected Electron-Phonon Coupling in Superconducting Pb Nanofilms Determined from He Atom Scattering. *Phys. Rev. Lett.* **2011**, *107*, 095502.

(21) Benedek, G.; Manson, J. R.; Miret-Artés, S. The Electron−Phonon Interaction of Low- Dimensional and Multi-Dimensional Materials from He Atom Scattering. *Adv. Mater.* **2020**, *32*, 2002072.

(22) Benedek, G.; Manson, J. R.; Miret-Artés, S.; Ruckhofer, A.; Ernst, W. E.; Tamtögl, A.; Toennies, J. P. Measuring the Electron-Phonon Interaction in Two-Dimensional Superconductors with He Atom Scattering. *Condens. Matter* **2020**, *5* (4), 79.

(23) Benedek, G.; Manson, J. R.; Miret-Artés, S.; Schmicker, D.; Toennies, J. P. Electron-Phonon Interaction in Non-Stoichiometric $Bi_2Sr_2CaCu_2O_{8+\delta}$ Superconductor from the Diffuse Elastic Helium Atom Scattering. *Condens. Matter* **2024**, *9*, 51.

(24) Xu, X.; Yang, W.; Song, H.; Wang, J.; Yu, L.; Ren, Z.; Liu, B. Structural sequence and superconductivity in high-entropy Mo-W-Re-Ru-Pd alloys. *Scr. Mater.* **2024**, *243*, 115986.

(25) Okada, M.; Baddorf, A. P.; Zehner, D. M. Hydrogen adsorption on Mo_{1-x} Re_x(110) (x = 0−0.25) surfaces. *Surf. Sci.* **1998**, *410*, 237−249.

(26) Ashcroft, N. W.; Mermin, N. D. *Solid State Physics*; Holt Saunders Int.: Philadelphia, 1976.

(27) Vesti, A.; Music, D.; Olsson, P. A. T. First-principles study on thermal expansion of W-Re sigma and chi phases. *Nucl. Mater. Energy* **2024**, *39*, 101684.

(28) Manson, J. R.; Benedek, G.; Miret-Artés, S. Atom scattering as a probe of the surface electron-phonon interaction at conducting surfaces. *Surf. Sci. Rep.* **2022**, *77*, 100552.

(29) Berge, S.; Gartland, P.; Slagsvold, B. J.; Slagsvold, B. J. Photoelectric work function of a molybde-num single crystal for the (100), (110), (111), (112), (114) and (332) faces. *Surf. Sci.* **1974**, *43*, 275−292.

(30) Ernst-Vidalis, M.-L.; Bauer, E. Hydrogen on Mo(ll0): Adsorption and Electron Stimulated H^+ Desorption. *Surf. Sci.* **1989**, *215*, 378.
(31) Robichaud, J.; Girouard, F. E. Thermionic work function of low index planes of rhenium. *Can. J. Phys.* **1980**, *58*, 43.
(32) Comsa, G.; Gelberg, A.; Iosifescu, B. Temperature Dependence of the Work Function of Metals (Mo,Ni). *Phys. Rev.* **1961**, *122*, 1091−1100.
(33) Kohler, B.; Ruggerone, P.; Wilke, S.; Scheffler, M. Frustrated H-Induced Instability of Mo(110). *Phys. Rev. Lett.* **1995**, *74*, 1387.
(34) Yakovkin, I. N.; Petrova, N. V.; Sologub, S. V.; Bordeniuk, I. V.; Amirov, R. H. Fermi surface of the H/Mo (110) adsorption system and related peculiarities in magneto- resistance. *Surf. Sci.* **2020**, *695*, 121572.
(35) Tulina, N. A.; Zaitsev, S. V. Point-Contact Spectroscopy Study of Quasilocal Vibrations in Molybdenum-Rhenium Alloys. *Solid State Commun.* **1993**, *86*, 55.
(36) Benedek, G.; Toennies, J. P. *Atomic-Scale Dynamics at Surfaces—Theory and Experimental Studies with Helium Atom Scattering*, Springer-Nature, 2018, Chapter 9.
(37) McMillan, W. L. Transition temperature of strong-coupled superconductors. *Phys. Rev.* **1968**, *167*, 331.
(38) Grimwall, G. *The Electron-Phonon Interaction in Metals 15*; North-Holland: Amsterdam, 1981.
(39) Ho, C. Y.; Powell, R. W.; Liley, P. E. Thermal Conductivity of the Elements: A Comprehensive Review. *J. Phys. Chem. Ref. Data* **1974**, 3 (1), 1.
(40) Sklyadneva, I. Yu.; Benedek, G.; Chulkov, E. V.; Echenique, P. M.; Heid, R.; Bohnen, K.-P.-.; Toennies, J. P. Mode-Selected Electron-Phonon Coupling in 31Superconducting Pb Nanofilms Determined from He Atom Scattering. *Phys. Rev. Lett.* **2011**, *107*, 095502.
(41) Braun, J.; Ruggerone, P.; Zhang, G.; Toennies, J. P.; Benedek, G. Surface Phonon Dispersion Curves of Thin Pb Films on Cu(111). *Phys. Rev. B* **2009**, *79*, 205423.
(42) Kohler, B.; Ruggerone, P.; Scheffler, M.; Tosatti, E. Enhanced Electron-Phonon Coupling at the Mo and W (110) Surfaces Induced by Adsorbed Hydrogen. *Z. Phys. Chem.* **1996**, *197*, 193.
(43) Kröger, J.; Lehwald, S.; Ibach, H. Substrate surface phonons in the cases of saturated (1 × 1)H/Mo(110) and p(2 × 2)O/Mo(110): a critical comparison. *Surf. Sci.* **1998**, *402*, 496.
(44) Kröger, J.; Lehwald, S.; Ibach, H. Estimation of the electron-phonon coupling parameter of Mo(110)-H and W(110)-H. *Phys. Rev. B* **2004**, *69*, 201404.
(45) Kröger, J. Electron−phonon coupling at metal surfaces. *Rep. Prog. Phys.* **2006**, *69*, 899.
(46) Rignanese, G.-M.; Finazzi, M. An up-to-date theoretical account applied to quasi-1D systems may be found in Ma- razzi, E. First-principle investigation of Kohn anomalies and Peierls instabilities. In *Metallic Nanowires*; Université Catholique de Louvain, 2021; . http://hdl.handle.net/2078.1/thesis:30676.
(47) Lian, C.-S.; Si, C.; Duan, W. Unveiling Charge-Density Wave, Superconductivity, and Their Competitive Nature in Two-Dimensional $NbSe_2$. *Nano Lett.* **2018**, *18*, 2924−2929.
(48) Gabovich, A. M.; Voitenko, A. I.; Ekino, T.; Sugimoto, A.; Yoshida, D.; Saito, T.; Suan Li, M.; Szymczak, H. Coexistence of superconductivity and charge-density waves: evidence from tunneling studies. *Low Temp. Phys.* **2023**, *49*, 881−898.
(49) Bekaert, J.; Petrov, M.; Aperis, A.; Oppeneer, P. M.; Milošević, M. V. Hydrogen-Induced High-Temperature Superconductivity in Two-Dimensional Materials: The Example of Hydrogenated Monolayer MgB_2. *Phys. Rev. Lett.* **2019**, *123*, 077001.

https://doi.org/10.1021/acs.jpcc.5c04084
J. Phys. Chem. C 2025, 129, 17632−17642